How protons are seen by high energy hadrons[1)]

Ugo Amaldi

CERN, Geneva, Switzerland
Usp. Fiz. Nauk **124**, 651–683 (April 1978)

PACS numbers: 13.85.Dz, 14.20.Ei, 12.40.Cc

CONTENTS

1. Protons, Neutrons, Hadrons and Their Structure 328
2. A Simple Picture of Diffraction Scattering 329
3. Experiments on Total Cross Sections 332
   3.1 Good geometry transmission experiments 332
   3.2 Colliding beam experiments 332
   3.3 Results on total cross sections 335
4. Experiments on Elastic Scattering 335
   4.1 Scattering in the Coulomb region 335
   4.2 Scattering at intermediate momentum transfers 338
   4.3 Scattering at large momentum transfers 339
5. What Have We Learned From Hadron-Proton Scattering? 340
   5.1 Energy dependence of total cross-sections 340
   5.2 Elastic cross-sections and hadron-proton absorptiveness 341
   5.3 Diffraction scattering and hadron structure 342
References 343

1. PROTONS, NEUTRONS, HADRONS AND THEIR STRUCTURE

More than 99.9% of all matter is made up of protons and neutrons. The interaction among these particles is thus one of the most prominent features of the physical world. In the Thirties, after the discovery of the neutron, the study of the forces that bind protons and neutrons to form nuclei became the central problem of a new field of research: nuclear physics. The hope was that it could be possible to obtain from experiments a relatively simple form for the nuclear potential that acts among protons and neutrons. As often happens, the situation is today very different from the forecasts made forty years ago.

To study better the forces acting between nucleons (i.e., between neutrons and protons) physicists went on building machines capable of accelerating protons to higher and higher energies. In the collisions of these energetic protons with nuclei new particles were produced and nowadays the number of known particles is so large that nobody thinks they are to be considered "elementary" in the old sense of the word. This large proliferation has affected only the particles which feel the strongest among all the known forces, the nuclear interaction. Indeed the particles that are sensitive only to the much less strong electromagnetic and weak interactions can still be counted on the fingers of a single hand. The road to the study of the forces acting between nucleons has thus brought us two fundamental facts: there are hundreds of different types of particles that are created through strong interactions, and which feel them, but only a few particles are sensitive *only* to weak and/or electromagnetic interactions. The two classes of particles have been named "hadrons" and "leptons".

By scattering leptons on hadrons and leptons on leptons we have learned that while hadrons are extended in space with radii of the order of 10^{-13} cm, leptons look point-like to our present level of spatial resolution, which is of the order of 10^{-15} cm. This fact already suggests the possibility for hadrons to be composed of other more "elementary" point-like constituents. After all the same trend appeared in the past in passing from molecules to atoms, from atoms to nuclei and electrons and from nuclei to protons and neutrons. About fifteen years ago such a vague statement was made more precise by the discovery that all known hadrons could be understood as bound systems of two or three subnuclear particles, the "quarks". Nowadays we have strong arguments to think that there are at least four different types of quarks, named u-quark, d-quark, s-squark and c-quark; in terms of the electric charge of a photon, their charges are $+2/3$, $-1/3$, $-1/3$ and $+2/3$, respectively. In the quark model a proton is made up of two u-quarks and one d-quark, while a neutron is made of

[1)]This English text has been supplied by the author, and is not being published in English elsewhere. It was translated into Russian for Usp. Fiz. Nauk by Yu. M. Antipov.

 0038-5670/78/040328-17$01.10

two d-quarks and one u-quark. Up to now nobody has ever seen a free quark, but the amount of information that can be correlated by making the hypothesis that hadrons behave as if they were made of quarks is so large that physicists have accepted to live with the following scheme: hadrons are made up of quarks but these constituents are prisoners within the hadrons themselves and they cannot be found as free particles. Not everybody is happy with this picture, but until free quarks are discovered this is the only viable description of the hadronic world.

Protons and neutrons are made of quarks bound together by quark-quark forces. The nuclear forces that bind protons and neutrons in nuclei are, in this scheme, residual forces among bound quarks similar to the Van der Waals forces acting between molecules. Also in the molecular case the simple Coulomb potential acting between nuclei and atomic electrons give rise to complicated forces between molecules. From this point of view the proton-proton, proton-neutron and neutron-neutron forces look much less interesting and fundamental than before. Still there are good reasons for studying the interactions of these particles. In fact one can consider protons as typical hadrons whose interactions can be studied in great detail due to the possibility of producing beams of intensity and energy that cannot be attained for other types of hadrons. Today the available beams of high energy protons are about a hundred thousand times more intense than the beams of any other hadron. Similarly, the energies available in the centre-of-mass for proton-proton collisions are more than five times larger than the corresponding quantity in any other hadron-hadron collision. One can thus say that proton-proton collisions are interesting not so much because about half of the mass of stable matter is contributed by protons, but because protons are typical hadrons and it is relatively easy to prepare very intense beams of high energy protons by separating electrons from hydrogen atoms and by accelerating the left-over nuclei.

Less intense beams of other hadrons can be produced by properly collimating and focussing the particles produced in the collisions of high energy protons with the nuclei of a target material. In the following we shall present data obtained with beams of antiprotons, positive and negative pions and positive and negative kaons. These particles differ by their presumed quark composition. Antiprotons (symbol $\bar{p}$) are the antiparticles of protons: they are formed of three antiquarks, usually indicated as $\bar{u}$, $\bar{u}$ and $\bar{d}$. Pions (symbol π) and kaons (symbol K) belong to a different family, the so-called bosons. They are bound states not of three but of two quarks, or more precisely of a quark and an antiquark. One can formally write the quark structure of the electrically charged particles, the only one that can be focussed in beams, as follows:

$$\pi^+ = u\bar{d}, \quad \pi^- = \bar{u}d; \quad K^+ = u\bar{s}, \quad K^- = \bar{u}s. \tag{1}$$

These four particles are metastable in the sense that they decay through weak interactions into other particles but their lifetime is long enough to be used many meters away from the production point. The study of their interactions complements very usefully the study of proton-proton collisions in spite of the smaller intensity and energy of the beams.

2. A SIMPLE PICTURE OF DIFFRACTION SCATTERING

If the energy of a hadron is larger than a few GeV (i.e. a few billion electronvolts), the nuclear forces acting between the projectile hadron and a hit target proton usually give rise to the production of other hadrons. We can say that when the two hadrons pass at distances of the order of 10^{-13} cm a localized burst of energy is produced that very often materializes so that a fraction of the energy transforms into the mass of a number of newly created particles. In these "inelastic" processes the rest of the energy appears as kinetic energy of the outgoing particles. In a relatively small percentage of the collisions no fraction of the available energy transforms into mass and the two hadrons suffer an "elastic" scattering.

The quantity which is best suited to express the energy at which a collision between two hadrons occurs is the energy available in the center-of-mass system, which will be indicated by the symbol $\sqrt{s}$. At any given center-of-mass energy, the probability of observing an elastic or an inelastic interaction when a moving hadron crosses a thin target is expressed by introducing the *elastic* and the *inelastic cross-sections*. These quantities are measured either in cm^2 or in millibarns ($1\ mb = 10^{-27}\ cm^2$) and can be defined as the equivalent target areas offered by one of the colliding hadrons to the other as far as elastic or inelastic processes are concerned. They depend both upon the type of the colliding hadrons and the energy in the center-of-mass. The total probability of interaction (which takes into account both elastic and inelastic processes) is obviously measured by the sum of the elastic and inelastic cross-sections. Introducing the symbols σ_{el} and σ_{in} to indicate the partial cross-sections, the *total cross-section* is then $\sigma_t = \sigma_{el} + \sigma_{in}$.

In the case of elastic collisions the important quantity is the distribution of the scattering probability as a function of the angle at which the projectile hadrons are scattered. Considering, for simplicity, proton-proton collisions in the center-of-mass system, the two protons of mass M which collide have a total energy $\sqrt{s}/2$ and momentum

$$p = \sqrt{\frac{s}{4c^2} - M^2c^2}. \tag{2}$$

If energy is measured in GeV, momentum is measured in GeV/c. Indicating by θ the scattering angle in the center-of-mass system, the *momentum transfer* t is defined as

$$t = 2M^2c^2 - \frac{s}{2} + 2p^2\cos\theta = -2p^2(1-\cos\theta). \tag{3}$$

The last expression is valid when the center-of-mass energy $\sqrt{s}$ is much larger than the rest energy of a proton, Mc^2. In the case of small angle scattering the momentum transfer simplifies further to

$$t \approx -p^2\theta^2. \tag{4}$$

For most of the data to be reviewed in this article, Eq. (4) is a good approximation so that one can say that the momentum transfer is proportional to the square both

of the momentum p and of the scattering angle θ.

In a hadron-proton collision, the distribution of the scattered hadrons is defined by the *differential cross section* $d\sigma/dt$, that is related to the cross section $d\sigma/d\Omega$ to find a scattered hadron in the solid angle $d\Omega$ by the expression

$$\frac{d\sigma}{dt}=\frac{\pi}{p^2}\frac{d\sigma}{d\Omega}. \tag{5}$$

Of course the integral of $d\sigma/d\Omega$ over the full solid angle gives back the elastic cross-section σ_{el}.

We have thus defined the main quantities measured and discussed in the field to be reviewed. They are: σ_t, σ_{el}, σ_{in} and $d\sigma/dt$. While introducing their definitions we have used a classical language which tacitly assumes that protons are tiny billiard balls that, in elastic collisions, hit and ricochet away from one another. However, quantum mechanics tells us that this picture is wrong, because each moving hadron behaves more as a wave than as a small ball. The wavelength λ of this wave is related to the momentum p of the particle by the well-known relation due to de Broglie, which reads $\lambda=h/p$. Numerically, the value of the Planck constant is 1.2 when the wavelength λ is measured in fermis (10^{-13} cm) and the momentum p of the particle in GeV/c.

Before going on to describe the experimental data and their detailed interpretation, it is worthwhile looking at high energy hadron-hadron scattering from a simple and intuitive point of view that takes into account the wave properties of matter. The phenomenon of two hadron waves which move towards one another and interact is difficult to visualize. However, it is completely equivalent to the more intuitive problem of a single wave which inpinges on an absorbing object fixed in space. For simplicity, in Fig. 1 we consider a disc. The disc is absorbing because, as discussed above, the interacting hadrons give rise to many inelastic processes which have the effect, in the wave description, of subtracting energy from the incoming wave and transferring it to the produced hadrons. The phenomenon can be characterized by the "profile function", which is the distribution of the absorption as a function of the distance from the center of the disc. In general this profile varies with the energy available in the center-of-mass, because the probability of the various inelastic processes is a function of the energy.

The far-reaching consequences of the wave nature of the interacting hadrons can be best appreciated by comparing the two simple situations depicted in Fig. 1. In Fig. 1a a large number of point-like particles move along parallel paths and are absorbed by a disc of radius R, while in Fig. 1b a plane wave is absorbed by a disc of equal radius. In the first case all particles hitting the disc are absorbed as a consequence of the inelastic processes in which other hadrons are produced. The inelastic cross-section is clearly equal to the area of the disc ($\sigma_{in}=\pi R^2$) and a "hole" appears in the incoming beam and extends to infinite distances. Since the point-like particles behave independently and each of them is either absorbed or unaffected by the disc, there is no elastic scattering and $\sigma_{el}=0$. In the case of Fig. 1b the incoming plane wave describes a

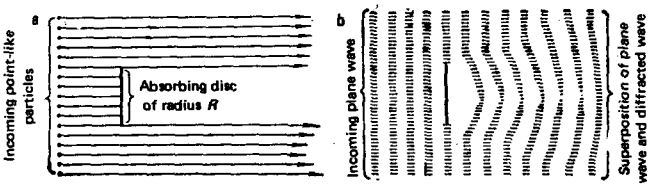

FIG. 1. (a) Classical description of the absorption of pointlike particles by a disc. The disc produces a hole in the flux of the impinging particles. (b) Wave description of the same phenomenon. The shadow is due to the superposition of two waves, the incoming unperturbed one and the diffracted wave.

beam of particles whose momentum can be deduced from the wavelength by means of the de Broglie relation. The portion of the wave front which strikes the disc is absorbed and its energy is converted into other forms of radiation emerging from the disc itself. These are the hadrons produced in the inelastic processes. In this case too the inelastic cross-section is $\sigma_{in}=\pi R^2$, but at the same time, due to the absorption, a "shadow" is generated behind the disc. At variance with the case of the "hole" produced in the beam of point-like particles, this shadow extends only to finite distances because the various portions of the wave front are *not* independent of each other. For this reason it is impossible to drill in the incoming wave a hole which remains as the wave travels to greater distances: the sharp edges of the hole in the wave front spread out sideways to fill the hole itself. Thus the very existence of absorption implies the appearance of a wave which has the same wavelength as the incoming wave and propagates from the disc outwards. This is the "diffracted" wave. It describes particles which are scattered *elastically* because they have the same wavelength as the incoming wave, and the momentum of the diffracted particles equals the initial momentum as a consequence of de Broglie relation.

How big is the elastic cross-section due to this diffraction phenomenon? For a completely absorbing disc of radius R, it is as large as the inelastic cross-section ($\sigma_{el}=\sigma_{in}=\pi R^2$), so that the total cross-section is *twice* the geometrical area of the absorbing disc. To accept this at first sight surprising result, it is necessary to understand how the shadow is formed. Two separate waves of the same wavelength propagate in space: the incident plane wave and the diffracted wave, which has spherical wave fronts because it has its source in the disc. The two waves interfere and, in particular, just behind the disc there must be totally destructive interference, so that the two amplitudes cancel and the shadow is produced. This requires the scattered wave to have behind the disc, and over an area equal to πR^2, the opposite phase but the same intensity as the incident wave. Thus the energy which is diffracted is equal to the energy which, transported by the incoming wave, impinges on the disc. This is turn implies that the elastic cross-section equals the inelastic one.

Summarizing, for a completely absorbing disc the elastic and inelastic cross-sections are equal, the total cross-section is twice the geometrical area, and thus the ratio $2\sigma_{el}/\sigma_t$ equals 1. For a disc of uniform but

not complete absorption the elastic cross-section becomes smaller in relation to the inelastic one, and it can be shown that the ratio $2\sigma_{el}/\sigma_t$, which is smaller than 1, is equal to the "absorptiveness", defined as the fraction A of the wave amplitude which is absorbed:

$$A=\frac{2\sigma_{el}}{\sigma}. \tag{6}$$

The proof of this result is very instructive. If the disc has uniform absorptiveness A, the amplitude behind the disc is reduced to a fraction $(1-A)$ of the incoming amplitude. Since here (as in optics) the intensity of the wave is proportional to the square of the amplitude, a fraction $(1-A)^2$ of the energy which impinges on the are πR^2 is transmitted. This implies that the fraction of this same energy which is absorbed is $1-(1-A)^2 = 2A-A^2$. The inelastic cross-section is then smaller than the area R^2 by the same factor: $\sigma_{in}=(2A-A^2)\pi R^2$. The value of the elastic cross-section is obtained by considering the intensity of the diffracted wave. In order to do so we use the principle enunciated for optical waves in 1837 by A. Babinet: the diffraction pattern due to any obstacle is equal to the pattern produced by the "complementary" screen, that is by the screen which is opaque where the obstacle is transparent and vice versa. The amplitdue of the wave behind the partially transparent hole of the complementary screen is A times the incoming amplitude, because it has to be the complement of the situation where the amplitude after the screen is reduced by the factor $(1-A)$. Then the intensity of the diffracted wave is proportional to A^2 and one has, for the complementary screen but also for the disc by virtue of the Babinet principle, $\sigma_{el}=A^2\pi R^2$. The total cross-section is $\sigma_t=\sigma_{in}+\sigma_{el}=2\pi R^2 A$, so that for complete absorption $(A=1)$ it equals twice the geometrical area of the disc. In general, by combining the expressions obtained for σ_{el} and σ_t, one obtains Eq. (6).

Summarizing, if diffraction scattering dominates, the ratio of the elastic to the total cross-section can be considered as a measure of the average "absorptiveness" of the colliding hadrons. The absorptiveness is determined by the many inelastic processes that can occur when the two hadrons collide, so that a measure of σ_{el} and σ_t tells us something concerning the inelastic processes that cause, through diffraction, the observed elastic scattering events. Of course the differential elastic cross-section $d\sigma/dt$ contains more information than the integrated cross section σ_{el}. Let us now discuss this point.

Detailed information on the absorptiveness profile is contained in the form of the diffraction pattern, that is, in the angular distribution of the scattered particles. This distribution presents a large maximum in the forward direction, at a scattering angle equal to zero, and a series of minima and maxima at larger angles, characteristic of all diffraction phenomena. In considering the angular width of the central peak of the diffraction pattern, it is enough to recall that in all diffraction phenomena the relevant quantity is the ratio between the wavelength and the dimensions R of the diffracting object. Thus the width of the central peak is proportional to the ratio λ/R, and from a measurement of the angular width the radius R can be obtained.

For an absorbing disc of radius R the distribution of the scattered intensity was derived in 1835 by G. B. Airy and is given by a well-known formula that in our present notation becomes:

$$\frac{d\sigma}{dt}=\left(\frac{d\sigma}{dt}\right)_{t=0}\left[\frac{2J_1(2\pi R\theta/\lambda)}{2\pi R\theta/\lambda}\right]^2\approx\left(\frac{d\sigma}{dt}\right)_{t=0}\exp\left[-\left(\frac{\pi R\theta}{\lambda}\right)^2\right]. \tag{7}$$

The Airy function reduces to a Gaussian in θ for small scattering angles.

Usually one parametrizes the forward differential hadron-hadron nuclear cross-section in the form

$$\frac{d\sigma}{dt}=\left(\frac{d\sigma}{dt}\right)_{t=0}e^{-b|t|}. \tag{8}$$

By recalling the de Broglie relation $\lambda=h/p$ and comparing Eqs. (7) and (8), the *slope* b of the forward elastic cross-section in a logarithmic plot versus $|t|$ is related to the *hadron-hadron interaction radius* R by the expression

$$b=\left(\frac{\pi R}{h}\right)^2\approx 6.5R^2 \tag{9}$$

To get a feeling for the orders of magnitude, an interaction radius of 1.4 fm, which is approximately the range of the nuclear forces, would give rise to a diffraction peak having a slope $b\simeq 13$ GeV^{-2}.

In conclusion, at high energy, hadron-hadron collisions are dominated by inelastic processes and the inelastic cross section $\sigma_{in}=\sigma_t-\sigma_{el}$ measures their probability. This implies a strong absorption of the incoming waves and thus diffraction scattering. The diffractive peak is expected to be an exponential in the momentum transfer and its slope b is proportional to the square of the interaction radius R. The integral σ_{el} of the differential cross-section is related to the absorption taking place within the radius R. More precisely, the ration $2\sigma_{el}/\sigma_t$ is a measure of the average absorptiveness. At this point a question arises very naturally: what is the meaning of the quantity $(d\sigma/dt)_{t=0}$, the only one for which no physical interpretation was given? The answer to this question may come as a surprise: the elastic cross-section at zero angle $(d\sigma/dt)_{t=0}$ is *not* an independent quantity as a consequence of the "optical theorem", which was put in precise mathematical form by Niels Bohr, Rudolf Peierls and George Placzek in 1936. This theorem is valid for all wave phenomena and for any absorptiveness profile. For simplicity we leave out its derivation. Here it is enough to indicate why one can expect such a theorem to exist. The wave nature of the interacting particles implies that *two* quantities determine the whole diffraction phenomenon: the interaction radius and the absorptiveness. On the other hand, from an experimental point of view, there are *three* quantities which are measured independently. They are usually the total cross-section, the forward elastic cross-section $(d\sigma/dt)_{t=0}$ and the slope b of the diffraction peak. (From these three quantities, all the others can be computed. For instance, the last two define the elastic cross-section σ_{el}, and the inelastic cross-section can be obtained as $\sigma_{in}=\sigma_t-\sigma_{el}$.) Quite naturally then, there is a relation among the three experimentally defined quantities. The proof shows that, indeed, the theorem relates only the first two of them, that is the forward cross-section and the total cross-section. But why does the forward elastic

cross-section play this very special role? This can be traced back to the fact that the plane incoming wave and the spherical diffracted wave are tangent to each other only in the forward direction, so that it is only there that the waves keep in step and are able to interfere at large distances from the absorbing disc.

With the present notation the optical theorem reads

$$\left(\frac{d\sigma}{dt}\right)_{t=0} = \frac{\pi}{4\hbar^2}\sigma_t^2. \tag{10}$$

As anticipated, the forward cross-section is not an independent quantity because it is proportional to the square of the total cross-section.

3. EXPERIMENTS ON TOTAL CROSS SECTIONS

3.1. Good geometry transmission experiments

In proton synchrotrons protons are accelerated to a maximum momentum, which is determined by the radius of the machine and the attainable maximum magnetic field in the magnets that keep the protons on their circular orbits. At the end of the acceleration cycle, a few seconds long, secondary particles are produced by bombarding with protons a target, placed either internally or externally with respect to the machine. The secondary particles produced in the forward direction are focussed and momentum analyzed in a beam transport system. The system used at Serpukhov by the IHEP-CERN collaboration a few years ago is sketched in Fig. 2, where the symbols K refer to collimators, L to quadrupole lenses and M to bending magnets.[1] S_1, S_2 and S_3 were scintillation counters defining the beam particles and A_1, A_2 were counters with a hole used in anticoincidence to reject halo particles. The detector W was used to optimize the focussing properties of the transport system. Various targets could be placed in the beam: hydrogen (H_2), deuterium (D_2), helium (He) and a dummy empty target (E) used for background subtraction.

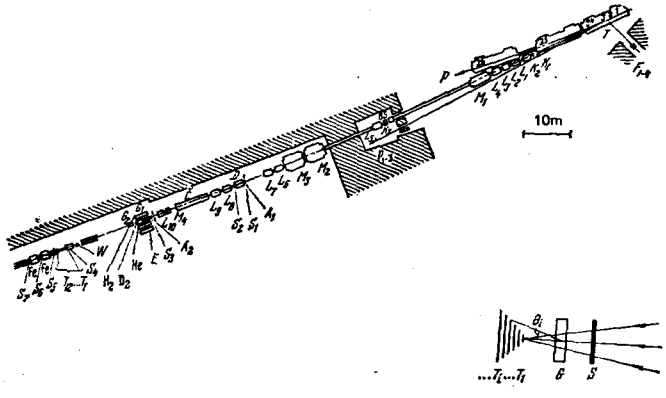

FIG. 2. System used at Serpukhov by the CERN-IHEP collaboration to measure total cross sections by the transmission technique. The particles produced in the target T by the proton circulating in the proton synchrotron are momentum analysed by a magnetic channel. The L and M refer to quadrupole lenses and to bending magnets respectively. K are collimators. Downstream of scintillator S_3 four targets could be placed in the beam. The inset shows the twelve transmission counters $T_1 \ldots T_{12}$ subtending increasing solid angles as seen from the target.

A differential Čerenkov counter (D) and a high resolution Čerenkov counter C were used to identify the particles, thus distinguishing electronically between pions, kaons and protons having the same momentum. These counters work on the principle of the Čerenkov effect: a particle of velocity v moving in a medium of index of refraction n emits light under an angle δ such that $\cos\delta = c/vn$.

Behind the target, twelve circular transmission counters ($T_1 \ldots T_{12}$), were mounted on a trolley which could move on rails along the beam line. At each momentum of the beam the trolley was moved so that the solid angle accepted a fixed range of momentum transfer: $|t| \leq 0.038$ (GeV/c)^2. In any experiment of this kind the rates measured in these counters are used to extrapolate to ideal conditions. Ideally one would like a beam of negligible transverse dimensions, a target without walls and one transmission counter, again of negligible transverse dimensions. Any hadron which interacts in the target would not be seen by the transmission counter, and the rate N measured by it would be smaller than the incident rate N_0 by a factor that depends exponentially upon σ_t. More precisely

$$\frac{N}{N_0} = \exp\left(-\frac{N_A \rho l}{P_A}\sigma_t\right), \tag{11}$$

where N_A is the Avogadro number, P_A is the atomic weight of the target, and ρl is the target thickness in g/cm^2. Since actual beams have finite dimensions, one is forced to use large transmission counters, which measure a slightly smaller value than σ_t. The total cross-section is then obtained by extrapolating to zero solid angle by using the rates measured in the twelve T-counters. Moreover, to take into account the scattering in the walls of the target, the rate N_0 is measured with a dummy target placed in the beam.

The details of the procedure used in this kind of good geometry measurements are discussed in the review paper by Giacomelli.[2] There it is shown that one can reach point-to-point errors which are as small as $\pm 0.1\%$.

3.2. Colliding beam experiments

Good geometry experiments produce among the most accurate measurements in hadronic physics. In 1971 a new type of accelerator came into operation at CERN, the Intersecting Storage Rings (ISR) in which two intense proton beams collide head-on. A completely new technique for measuring total cross-section had then to be invented. This is the second argument to be discussed in this section.

When a relativistic proton of laboratory momentum p_{lab} collides with a stationary proton of mass M, the center-of-mass (c.m.) energy has the form:

$$\sqrt{s} \approx \sqrt{2Mp_{\text{lab}}}. \tag{12}$$

It follows from the equation that in the collision of a proton of 26 GeV/c (close to the maximum momentum at which protons can be accelerated in the CERN proton-synchrotron) with a hydrogen nucleus the energy available in the c.m. is about 7 GeV. The rest of the energy is wasted, so to speak, due to the motion of the center-of-mass.

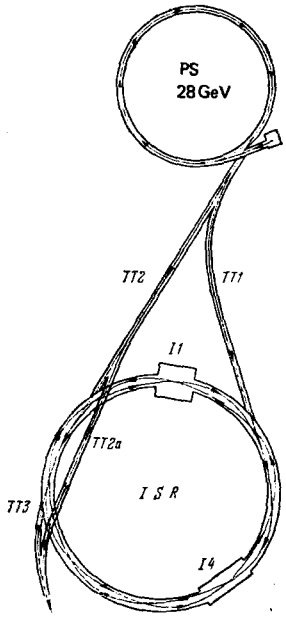

FIG. 3. Schematic drawing of the CERN protonsynchrotron (PS), that injects protons into the Intersecting Storage Rings (ISR) through two transfer tunnels (*TT*1 and *TT*2). The ISR diameter is 300 meters. The two proton beams stacked in the ISR cross in eight points. I1 and I4 are the largest experimental area built around the intersecting points number 1 and 4.

In the collision of two relativistic protons which have opposite and equal momenta p, the center-of-mass is fixed in the laboratory and the c.m. energy is simply

$$\sqrt{s} \approx 2p. \tag{13}$$

Combining Eqs. (12) and (13) one obtains the "equivalent" laboratory momentum p_{lab} of a collision in which both protons move in opposite direction with momentum p:

$$p_{\text{lab}} \approx \frac{2p^2}{M}.$$

For example, for two protons of momenta $p = 26$ GeV/c the equivalent laboratory momentum is $p_{\text{lab}} \simeq 1500$ GeV/c.

Thus the reason for constructing colliding beam machines is the very high c.m. energies that can be achieved. The CERN ISR is the first high-energy proton colliding beam facility to be built and produces the highest c.m. energies in the world. A general description was given by K. Johnsen.[3] As schematically indicated in Fig. 3, two storage rings cross at eight points and are filled with protons accelerated by the CERN Proton-Synchrotron (PS). In each ring the protons are bent by 132 strong focussing magnets. The beams circulate in two vacuum chambers which have a cross-section of 50 mm×200 mm and a diameter of 300 m, and cross in the horizontal plane in the eight interaction regions at an angle of 14.8°. During injection, every two or three seconds, a pulse of about $2 \cdot 10^{12}$ protons is injected into one of the two rings. Each ring is filled with about 200 pulses, so that, during normal operation, the number of protons in each ring is larger than $5 \cdot 10^{14}$. Since the revolution time is about 3 μs, this corresponds to a current of about 25A. The residual pressure in the vacuum chambers is so low (some units in 10^{-12} Torr) that the lifetime of the two beams is typically greater than one year! Excellent experimental conditions are therefore available for runs of many days.

The rms value of the beam height is of the order of 1.5 mm, while the width in the horizontal plane is determined by the momentum band accepted. With a typical momentum acceptance $\Delta p/p = 2\%$, the width is ~40 mm, so that the two beams can be visualized as two thin, wide ribbons which cross in the eight intersection regions at 14.8°. Due to this angle and to the horizontal width, the length of the collision source is ±150 mm, while, as noted above, its radial width in normal runs is of the order of ±20 mm. This radial width can be reduced by switching on special quadrupoles in the machine lattice, which, in four of the eight intersection regions, superimpose the trajectories of the protons having different momenta. When the "Terwilliger scheme" is on, the width of the beam is reduced to ~±5 mm and the length of the source becomes ~±40 mm. Special scraping procedures applied to the beams at injection and after stacking of the beams can reduce the length of the source to ±15 mm.

The luminosity L of two colliding beams is, by definition, the proportionality factor between a cross section $\Delta\sigma_x$ (for detecting events of type x in the solid angle of the apparatus) and the corresponding detection rate N_x.

$$N_x = L\Delta\sigma_x. \tag{14}$$

L is usually measured in units of cm^{-2} s^{-1}. The luminosity can be expressed as a function of the parameters which characterize the two crossing beams:

$$L(\delta) = \frac{I_1 I_2}{e^2 c \tan 1/2\gamma} \int_{-\infty}^{+\infty} \rho_1(z)\, \rho_2(z+\delta)\, dz. \tag{15}$$

In this expression I_1 and I_2 are the two proton currents, e is the electronic charge, c the velocity of light, $\gamma = 14.8°$ is the angle at which the two beams cross in the horizontal plane, ρ_1 and ρ_2 are the vertical distributions of the beams normalized to 1. The distributions are supposed to be centered around the vertical coordinates z_1 and z_2, and $\delta = z_1 - z_2$ is the vertical distance between the centres of the two beams. Of course the luminosity is a function of δ and, for bell-shaped vertical distributions, it is maximum for $\delta = 0$. The dependence of the luminosity on the product of the currents expresses the fact that L increases proportionally to the number of circulating protons in each ring. In Eq. (15) only the folding of the vertical distributions of the two currents appears because the two beams form an angle $\gamma \neq 0$ in the horizontal plane. This guarantees that the projection of the trajectories cross at one point, so that the horizontal distribution does not influence the luminosity.

Using the approximate figures quoted above ($\sigma \simeq 1.5$ mm), and average values for the currents ($I_1 = I_2 = 25$A) one obtains from Eq. (15):

$$L \approx 10^{31} \text{ cm}^{-2} \text{ s}^{-1}. \tag{16}$$

It is interesting to compare this luminosity with the luminosity which is obtained by directing a proton beam, extracted from a proton-synchrotron (~$5 \cdot 10^{12}$ proton s^{-1}), onto a hydrogen target 100 cm long:

$$L \approx 2.5 \cdot 10^{27} \text{ cm}^{-2} \text{ s}^{-1}. \tag{17}$$

It follows from the comparison that, as far as luminosity is concerned, the ISR is equivalent to a proton synchrotron beam traversing a hydrogen target which

is about 0.4 μm thick.

The accurate measurement of the luminosity is one of the most difficult problems in experimentation with colliding beams and, in particular, it is very important for the measurements of total cross-sections. At the ISR the luminosity measurements are performed by means of the Van der Meer method.[4] The method consists in vertically displacing the two beams in an intersection region by small, known steps by means of well-calibrated magnets producing a horizontal field. The counting rate $N_m(\delta)$ in a system of counters, which is used as a monitor, is measured for each displacement δ between the centers of the two beams. Combining Eqs. (14) and (15) one has

$$N_m(\delta) = \Delta\sigma_m \frac{I_1 I_2}{e^2 \operatorname{ctan} 1/2\gamma} \int_{-\infty}^{+\infty} \rho_1(z)\,\rho_2(z+\delta)\,dz. \tag{18}$$

From this expression it is immediately seen that, by integrating the measured monitor rate over the displacement δ, the double integral of the vertical distributions over dz and $d\delta$ reduces to 1 (because both ρ_1 and ρ_2 are normalized to 1) and one has

$$\Delta\sigma_m = \frac{e^2 \operatorname{ctan} 1/2\gamma}{I_1 I_2} \int_{-\infty}^{+\infty} N_m(\delta)\,d\delta. \tag{19}$$

Since the beam currents can be measured with very high precision, the cross section of the monitor system $\Delta\sigma_m$ (which is a function of the beam momenta) is obtained with a percentage error equal to the one involved in the measurement of the monitor rate $N_m(\delta)$ and in the calculation of the integral. Careful studies and controls of the errors involved in the knowledge of the beam displacement , made by the ISR machine group, the CERN-Rome Collaboration, and the Pisa-Stony Brook Collaboration, have led to the conclusion that the scale of displacements is known today (1977) within an absolute accuracy of $\pm 0.5\%$.[5] Since typical steps in the luminosity measurements are $\Delta\delta = 0.5$ mm, this corresponds to an error in this displacement of ± 0.0025 mm. The point-to-point errors on $\Delta\sigma_m$ depend upon the long-term stability of the monitor counters and on the reproducibility of the vertical displacements of the beams. The standard deviation of $\Delta\sigma_m$ obtained by the CERN-Rome Collaboration and the Pisa-Stony Brook collaboration is $\pm 0.5\%$. Once the monitor cross-section $\Delta\sigma_m$ is known for a given momentum of the circulating protons, the luminosity L can be obtained by measuring the monitor rate N_m per second and by applying Eq. (14).

The two groups already mentioned have performed extensive measurements of the total proton-proton cross section at the ISR. In 1973 they discovered the ~10% rise of σ_t in the energy interval $22 \leq \sqrt{s} < 63$ GeV.[6,7] Recently the accuracy of the measurements has been greatly improved by using the apparatus sketched in Fig. 4.[5,8] Two different methods have been applied by the CERN-Rome and by the Pisa-Stony Brook Collaborations.

The CERN-Rome method used the hodoscopes A and B placed at small angles with respect to the circulating protons and can logically be described as follows:

i) measurement of the elastic rate $N_{el}(\theta)$ in a known solid angle $\Delta\Omega$ at some small scattering angle θ (5 mrad in this experiment);

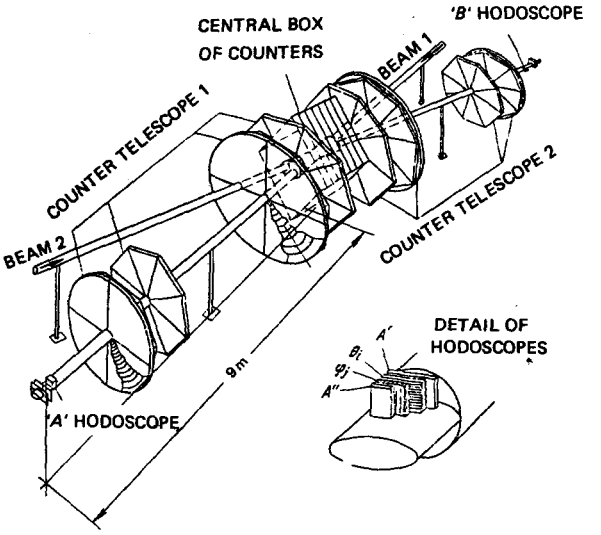

FIG. 4. Perspective view of the CERN-Pisa-Rome-Stony Brook experiment to measure total cross sections at the ISR. The two beam pipes cross at an angle of 14.8°. The eight big wheels represent the large hodoscopes used to detect the total number of proton-proton interactions. The hodoscopes *A* and *B*, whose details appear in the inset, were used to detect the protons elastically scattered at small angles ($\theta \simeq 5$ mrad) and thus to obtain the total cross section by applying the CERN-Rome method.

ii) extrapolation of the elastic rate, with the usual exponential behavior with respect to t of Eq. (8), to zero angle to obtain $N_{el}(0)$;

iii) application of Eq. (14) to deduce the elastic cross-section in the forward direction:

$$\left(\frac{d\sigma}{d\Omega}\right)_{t=0} = \frac{N_{el}(0)}{L\,d\Omega};$$

iv) use of the optical theorem to derive σ_t [(Eqs. (10) and (5)]. In terms of quantities directly measured

$$\sigma_t = \frac{2h}{\rho} \sqrt{\frac{1}{L} \frac{N_{el}(0)}{\Delta\Omega}}. \tag{20}$$

The Pisa-Stony Brook Collaboration, that used the large apparatus of about 500 counters, appearing as big wheels in Fig. 4, detected the total number of proton-proton interactions over a large fraction of the whole solid angle. From this measurement the rate N_t, extrapolated to the whole solid angle, was obtained, and the total cross-section was deduced by applying Eq. (14):

$$\sigma_t = \frac{N_t}{L}. \tag{21}$$

The extrapolation (which is of the order of 5%) is mainly needed to correct for elastic events which are unavoidably lost because the charged particles do not come out of the vacuum chamber.

In the approaches used by the CERN-Rome and the Pisa-Stony Brook Collaborations, the total cross-section depends in different ways on the luminosity L: in one case $\sigma_t \propto L^{-1/2}$ [Eq. (20)] while in the other $\sigma_t \propto L^{-1}$ [Eq. (21)]. It is thus possible to combine the two methods and to obtain a value of the cross section which

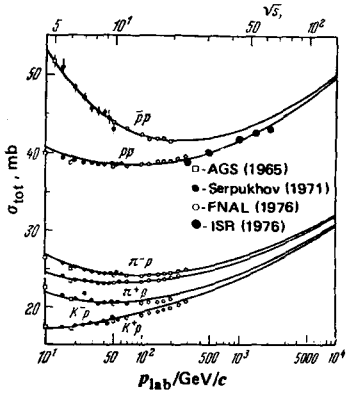

FIG. 5. Compilation of data on total cross section as a function of the laboratory momentum of the incident hadron p_{lab} and of the total energy in the center of mass $\sqrt{s}$. The curves are from a model by Lipkin, to be discussed in Section 5.1.

does not depend upon the luminosity of the colliding beams. This technique has been recently used by the two collaborations already working in the field. Data have been taken simultaneously with the experimental arrangements of Fig. 4, so that elastic and inelastic rates were measured for the same machine luminosity and the total cross section was derived by applying the formula

$$\sigma_t = \frac{4\hbar^2}{p^2}\frac{N_{el}(0)}{N_t}\frac{1}{\Delta\Omega}. \qquad (22)$$

The results of the three methods are perfectly consistent, and the point to point error of the combined results is ±0.6%. The scale error of this weighted average is ±0.7%.[5]

3.3. Results on total cross sections

The available data on total cross sections for protons[1,5,9,10,11] are summarized in Fig. 5. The meaning of the curves will be discussed in Sec. 5.1. The inelastic cross sections of Fig. 6 have been obtained by subtracting from σ_t the elastic cross-sections σ_{el}, that will be discussed in the next section. The differences

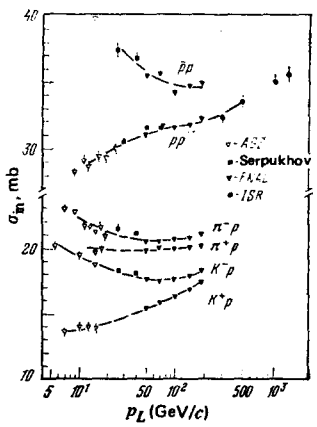

FIG. 6. Momentum dependence of the inelastic cross section defined as $\sigma_{in}=\sigma_t-\sigma_{el}$. Note that σ_{in} increases steadily with p_{lab} only for the two channels K^+p and pp. This is attributed to the quark composition of the two interacting hadrons: only for these two channels there is no pair of quarks that could annihilate in the interaction. In fact the quark composition of a K^+ and a proton are $u\bar{s}$ and uud respectively [see Eq. (1)]. On the other hand a π^+, for instance, has the composition $u\bar{d}$, and the $\bar{d}$ can annihilate with the d-quark in the proton target.

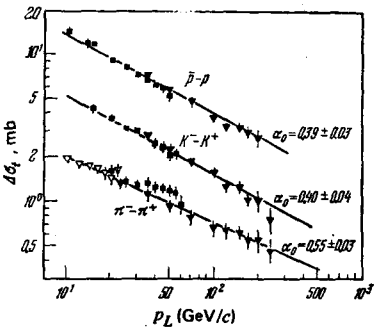

FIG. 7. Differences between the total cross-section of negative and positive particles on protons: $\Delta\sigma_t=\sigma_t^- - \sigma_t^+$. The data have been fitted with a power dependence, as expected in a Regge exchange model (see Section 5.1). The parameter α_0 is defined by $\Delta\sigma_t=\sigma_0\cdot p_L^{-\alpha_0}$.

in σ_t for negative and positive particles are plotted versus the laboratory momentum in Fig. 7. The interpretation of these data will be discussed after some typical experiments on elastic scattering have been presented.

4. EXPERIMENTS ON ELASTIC SCATTERING

4.1. Scattering in the Coulomb region

Until now we have, for simplicity, neglected the fact that two charged hadrons scatter not only through the nuclear interaction, but also because their electric charges repel or attract each other as a result of the Coulomb force. Since the two types of scattering cannot be distinguished, quantum mechanics tells us that one has to sum the two amplitudes and that the differential cross section contains an interference term. At high energy and in the forward direction the nuclear amplitude f_N is, as we have seen, mainly diffractive. Formally this means that its phase differs by $\pi/2$ with respect to the phase of the Coulomb amplitude f_C. Since the amplitude due to real Coulomb potential is real, it follows that the nuclear amplitude is mainly imaginary. However, in general it contains a small real part, which for reasons of simplicity we have neglected until now. To be consistent with the exponential parametrization in $|t|$ [Eq. (8)] and with the optical theorem [Eq. (10)] one usually writes:

$$f_N=(i+\rho)\frac{\sigma_t}{2\hbar}e^{-b|t|/2}. \qquad (23)$$

With this normalization the differential cross section takes the form $d\sigma/dt=\pi|f|^2$. In the diffractive regime the *ratio ρ between the real and the imaginary part of the nuclear amplitude* is expected to be much smaller than 1. The amplitude due to the Coulomb potential is well known: for point-like particles of equal elementary charges

$$f_C=-\frac{\alpha}{\pi}\frac{\hbar}{p\beta\theta^2}, \qquad (24)$$

where $\alpha=1/137$ is the fine structure constant. Eq. (24) gives the celebrated $1/\theta^4$ angular dependence of the Rutherford elastic cross section. To complete it, small corrections have to be applied to take into account the finite dimensions of the hadrons and the effect of a small imaginary part.

By summing the two amplitudes and then squaring, the elastic differential cross section becomes

$$\frac{d\sigma}{dt} = \pi f_N^2 + \pi f_C^2 - \frac{\alpha}{|t|}\rho\sigma_t e^{-b|t|/2} + \text{small corrections}. \quad (25)$$

The third term is due to the interference between the two amplitudes and has a different angular dependence: it is proportional to $1/\theta^2$. This allows its separation and thus the determination of the ratio ρ of the real to the imaginary part of the nuclear amplitude, once σ_t and b are known. Eq. (25) is the basis of all experiments which, by measuring $d\sigma/dt$ in the region where the interference is not negligible, derive the ratio ρ. The interference is greatest where the nuclear and Coulomb amplitudes are equal, that is at momentum transfers $t \simeq 2 \cdot 10^{-3}$ GeV^2. These small values of t, the so-called "Coulomb region", have to be reached to measure ρ. In the following we shall describe two types of experiments performed one at Serpukhov and at the Fermilab proton synchrotron, and the other at the Intersecting Storage Rings.

V. Nikitin and coworkers at the Joint Institute for Nuclear Research in Dubna were the first to study proton-proton scattering at small momentum transfers by measuring the kinetic energy of the recoil proton.[12,13] After a projectile proton has been scattered by a proton at rest in the laboratory, the fast proton moves at a small angle θ in the laboratory while the other proton recoils at angles around 90° with a small kinetic energy T. This kinetic energy is directly proportional to the momentum transfer:

$$|t| = 2MT. \quad (26)$$

The experimental method is based on the measurement of T. Since the range of these protons is very small, one must use thin targets. The group mentioned above, together with Y. Pilipenko, devised a supersonic hydrogen jet as a target to be put in the internal beam of an accelerator. The first experiment was performed at Serpukhov[14] and the others at Fermilab near Chicago.[15]

A schematic layout of the detection apparatus is shown in Fig. 8. The beam circulating in the accelerator traverses the gas jet pre-cooled at 40° K and the recoil protons are detected at a distance of about 2.5 m

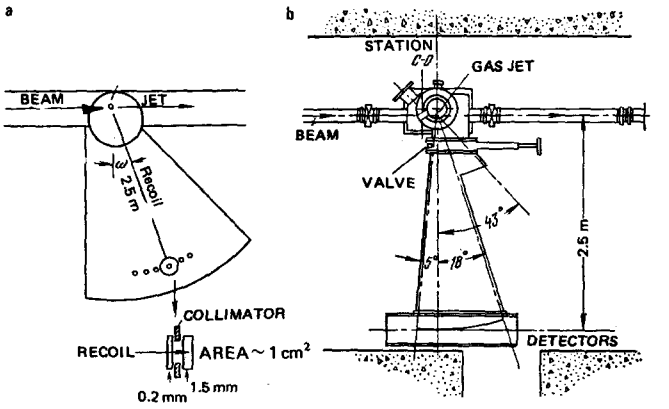

FIG. 8. (a) Principle of the gas jet technique. The circulating proton beam of a synchrotron traverses the jet of hydrogen, which moves perpendicularly to the drawing. The recoil proton is detected at few meters by solid state detectors. In some cases the sensitive area of the detectors is reduced by means of a collimator. (b) Realization of the above principle. A valve is used to separate the vacuum in the accelerator from the chamber containing the detectors.

by detectors mounted on a moveable carriage. Many solid state detectors of ~1 cm² area measure the proton energies, if these are smaller than about 30 MeV. Since each detector is located at a fixed angle, the energy spectrum of the recoils registered by the detector shows a peak for elastically scattered protons. This allows a very accurate subtraction of the events due to the nonelastic background. In this experiment the high intensity of the internal beam and the multiple traversals through the target compensate for the small density of the hydrogen jet and result in luminosities of the order of 10^{34} cm^{-2} s^{-1}. However, it is very difficult to measure absolute cross sections because an independent measurement of the beam-jet luminosity cannot be performed.

The second experiment to be discussed was performed by the CERN-Rome Collaboration at the Intersecting Storage Rings.[16,17] A sketch of the experimental arrangement is shown in Fig. 9. Protons elasti-

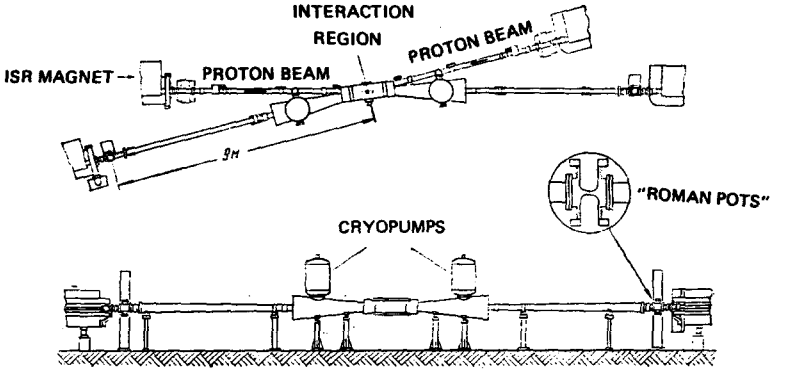

FIG. 9. Plan view and side view of one of the ISR interaction regions where a Coulomb experiment has been performed. Two columns placed at 9 meters from the crossing point hold two movable indents of the vacuum chambers. These so called "Roman pots" were moved very close to the circulating beams after their stacking in the machine was completed.

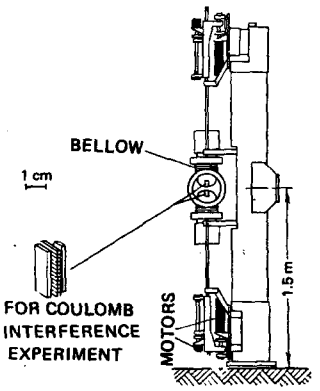

FIG. 10. Mechanical mounting of one column and two Roman pots. One of the two motors below moves the lower pot, the other moves the hodoscope system in the pot. For the Coulomb experiment performed in the years 1972-1973[16] each of the four hodoscopes was formed of 14 scintillators and had the structure indicated in the figure. In the last refined experiment, performed in 1976-1977[16], each hodoscope was formed of 32 scintillators.

cally scattered in the vertical plane were detected by hodoscopes of scintillators placed in indents of the vacuum chamber at about 9 m from the intersection point. The movable sections are known by now as "Roman pots". A cross section of the holding column, with Roman pots and a hodoscope is shown in Fig. 10. Four scintillator hodoscopes were placed in these pots, which were moved very close to the circulating beams after the stacking of the protons was completed. Successively the scintillators were moved inside the pots to come as close as possible to the circulating beams. The hodoscopes were assembled in three layers; a stack of twenty four 2 mm high scintillators that defined the vertical component of the scattering angle, an array of seven vertical 4 mm wide fingers that determined the horizontal component, and behind them a single trigger counter. The four hodoscopes were combined in two pairs such that, for elastic collisions, if one proton hit a hodoscope the other proton traversed the hodoscope conjugate to the first one.

To be able to move the counters well into the region where Coulomb scattering dominates, beams of a height and a width of only a few mm were essential. Therefore the ISR was operated using the Terwilliger focussing scheme, described in Section 3.2, and thus superimposing the equilibrium orbits for different momenta in the intersection region. In addition the halos of the beams were scraped off at injection time and at regular intervals during data taking. Beams of a few ampères were obtained with cross sections twice as low and ten times as narrow as under normal running conditions. This made it possible to bring the counters as close as 9 mm from the beam axis, where they detected protons scattered at angles of 1 mrad.[16] This corresponds to $|t| \simeq 10^{-3}$ GeV^2 when the momentum of the two colliding beams is 31 GeV, the maximum attainable at the ISR.

A typical angular distribution obtained at 26.7 GeV is shown in Fig. 11. At small values of the momentum transfer the rapid decrease of the Coulomb cross sec-

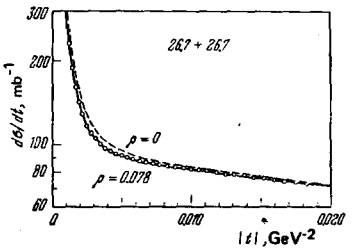

FIG. 11. Typical differential cross section measured at the CERN ISR. At very small momentum transfers the Coulomb amplitude dominates, while above $|t| \simeq 0.01$ the nuclear amplitude determines the behavior of the cross section. The continuous line represents the best fit to the data.

tion is apparent. Above $|t| \simeq 0.01$ GeV^2 the slowly decreasing nuclear amplitude dominates. The dashed line represents the expected distribution if the ratio ρ between the real and the imaginary parts was zero. It is seen that the interference is destructive. A fit to the data gives $\rho = 0.078 \pm 0.010$. This is one of the most accurate measurements ever performed of the quantity ρ.

Fig. 12 is an up-to-date summary of the available information on ρ obtained with the usual six types of projectile hadrons.[15,16,17] At momenta of the projectile hadrons larger than a few GeV/c, ρ is of the order of 10^{-1}, i.e. the elastic scattering amplitude is essentially imaginary as is expected for a diffractive amplitude.

In optics the real part of the refractive index of a medium at a given frequency may be expressed as an integral over a function of the imaginary part of the refractive index extended to all frequencies. Such a "dispersion relation" follows from a very simple causality condition; when a light packet impinges on a medium, no diffracted wave can appear before the packet arrives. Of course the same condition applies to the quantum mechanical wave packets describing the hadrons. Thus a dispersion relation connects the real

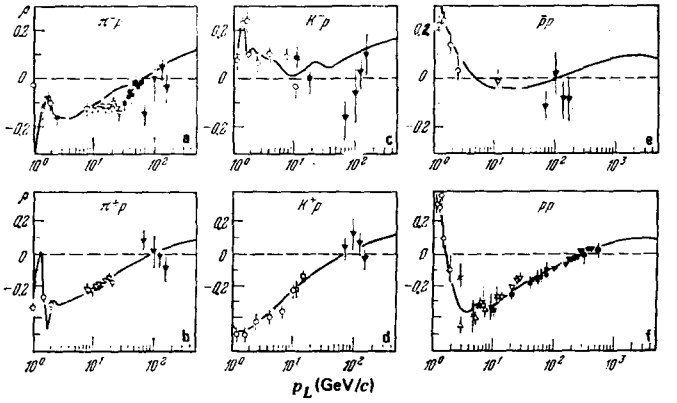

FIG. 12. The data for this compilation of the ratio ρ between the real and the imaginary part of the forward nuclear amplitude have been taken from Refs. 15, 16, and 17. The curves are computed by means of dispersion relations by using as input the total cross section.[18] The overall agreement is good.

and the imaginary parts of the nuclear amplitude. Since the imaginary part of the nuclear amplitude is proportional to the total cross section (optical theorem), at any given energy the value of ρ may be expressed as an integral of the total cross sections for particle and antiparticle over the whole energy region. The curves of Fig. 12 have been computed in this way[18] and their overall agreement with the data demonstrates the validity of the causality principle in the subnuclear world.

4.2. Scattering at intermediate momentum transfers

As discussed towards the end of section 2, the measurement of the forward slope b of the nuclear differential cross section is equivalent to a determination of the hadron-hadron interaction radius. (In this connection it is worth looking back to Eq. (9).) Indeed, according to the indeterminacy principle, collisions with small momentum transfers probe large spatial distances, and they give information not on the internal structure of the hadrons but on their overall dimensions and shape. This was the aim of an experiment now being performed at Fermilab by the Single Arm Spectrometer Group.[19]

This experiment used particles of momenta between 20 and 200 GeV/c produced in a beryllium target at 2.65 mrad with respect to the extracted proton beam from the 400 GeV accelerator. The beam transport system had three stages each 150 m long: a collection stage, in which the solid angle and momentum bite were defined, a filtering stage, which suppressed the beam halo, and a recombination stage, which produced the final achromatic image. Along the transport system hodoscopes of scintillators measured the momentum and the direction of the incident particles and Čerenkov counters tapped it as a pion, a kaon or a nucleon. At the end of the transport system there was the hydrogen target followed by the spectrometer. Since the spectrometer was situated at 0° with respect to the transport system, it could not pivot around the target to vary the scattering angle. The angle between the incident beam and the spectrometer was then varied by magnetic deflection of the incident beam. A system of three bending magnets located just upstream of the hydrogen target was used to pitch the incident beam in the vertical plane, as shown in Fig. 13. Along the spectrometer, ten multiwire proportional chambers provided information about the trajectory and the momentum of the scattered particles. Three threshold Čerenkov counters and a differential Čerenkov counter served to identify scattered particles as pions, kaons or nucleons.

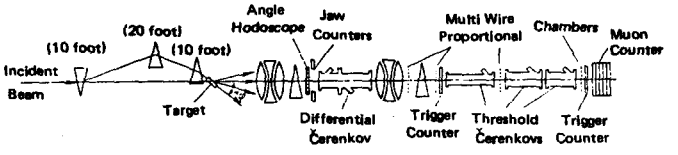

FIG. 13. Schematic drawing of the Single Arm Spectrometer at Fermilab. The incident beam is deflected in the vertical plane so that the spectrometer detected particles scattered in the target at the angle ϕ. Multiwire proportional chambers measured the scattered particles and four Čerenkov counters identified them.

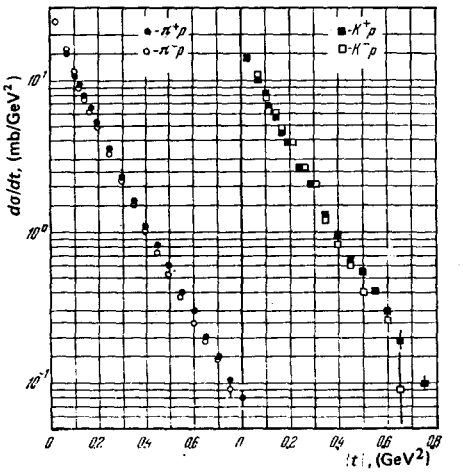

FIG. 14. Differential cross section versus the momentum transfer at $p_{lab} = 175$ GeV/c. A similar behavior is observed also at the other momenta measured by the Single Arm Spectrometer Group.[19] The data are well fitted by the parametrization of Eq. (26).

Some of the data obtained in this experiment are shown in Fig. 14. The qualitative behaviour of the angular distribution is similar for all projectile hadrons at all momenta. For $|t| \lesssim 0.8$ GeV^2 all the data can be well fitted by the simple expression

$$\frac{d\sigma}{dt} = \left(\frac{d\sigma}{dt}\right)_{t=0} \exp(-B|t| + Ct^2), \qquad (26)$$

where C is of the order of 2 GeV^{-4} above 10 GeV/c. The quadratic term is introduced to reproduce the concave behavior of $d\sigma/dt$ appearing in Fig. 14. For $|t|$ smaller than 0.1 GeV^2 the second term in the exponential is negligible and the parameter B measures the interaction radius. Figure 15a summarizes the present-

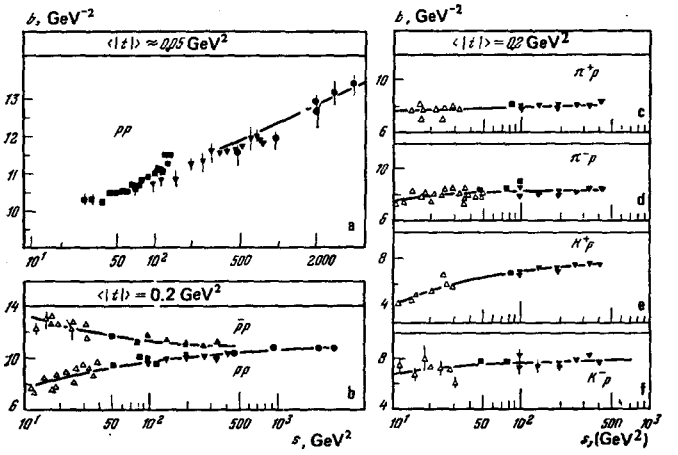

FIG. 15. Compilation of slope data.[16,20] Since the slope of the differential cross section depends upon the differential cross section depends upon the momentum transfer, the average value of $|t|$ has to be specified. Figure a shows the logarithmic increase of the proton-proton slope at a very small value of the momentum transfer. The other figures show the energy dependence of the slope of the usual six scattering reactions for a larger value of the momentum transfer. The larger increase is observed in the pp and in the K^+p channels, reminiscent of the situation found for the inelastic cross section (Fig. 6).

ly available data on the slope b of proton-proton scattering.[20] The forward slope increases logarithmically with s, the square of the centre of mass energy.

An educated fit to the data above 100 GeV^2 is:

$$b_{pp} = 6.97 + 0.77\sqrt{\ln(s)} \qquad (27)$$

This increase of the slope is usually expressed by saying either than "the forward proton-proton nuclear amplitude shrinks with energy" or that "the proton-proton interaction radius increases logarithmically with energy". A similar behavior is observed in the K^+p channels, while the diffraction peaks in π^+p and K^-p scattering do not shrink appreciably with energy.

Figure 15 also shows the energy dependence of the slopes measured at an intermediate value of the momentum transfer, $|t| = 0.2$ GeV. There is less energy dependence at this transverse momentum than at $|t| \approx 0$.

4.3. Scattering at large momentum transfers

The Aachen-CERN-Geneva-Harvard-Torino Collaboration working at the CERN Intersecting Storage Rings (ISR) discovered that at high energy the proton-proton differential cross section has a minimum around $|t| = 1.4$ GeV^2. Figure 16 summarizes the data as a function of the momentum of the projectile proton impinging on a proton at rest in the laboratory.[21] The typical diffractive minimum is deepest around 200 GeV/c and moves towards smaller values of $|t|$ when the energy increases. This behavior is consistent with the shrinkage of the forward slope: in the ISR energy range, that is for $\sqrt{s}$ increasing from 23 to 63 GeV, the slope b increases by $(12 \pm 3)\%$, while the value of the momentum transfer $|t_m|$, at which the minimum appears, decreases by $(14 \pm 3)\%$.[22] These two facts are both consistent with a proton-proton interaction radius increasing with energy by about 6% in the ISR energy range, which corresponds to a range of laboratory momentum which goes from 290 to 2000 GeV/c.

Recently further data have been obtained by the CERN-Hamburg-Orsay-Vienna Collaboration.[23] This group has worked for many years using the Split Field Magnet (SFM) mounted in one of the intersection regions

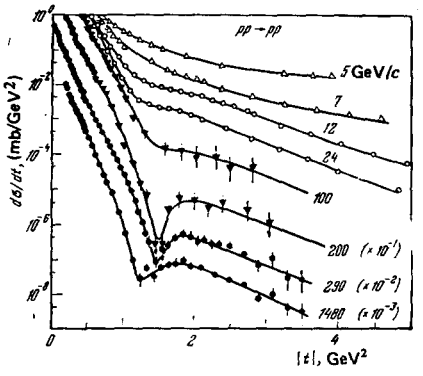

FIG. 16. The dip in proton-proton elastic scattering gets deeper with the momentum of the incoming proton. Moreover the position of the diffractive minimum moves with momentum towards smaller momentum transfers. The data are taken from from the papers of Ref. 21 and 22.

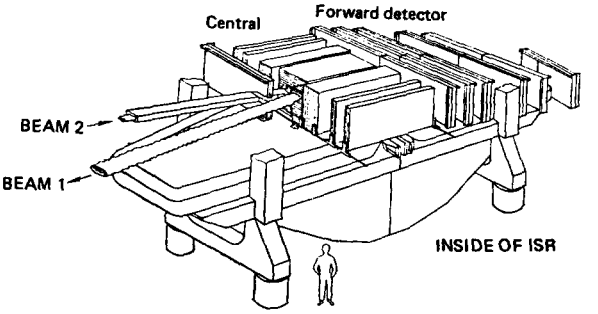

FIG. 17. Perspective view of the Split Field Magnet (SFM) mounted in intersection 4 of the ISR. The top part of the magnet and the forward detector on beam 1 are removed to show the details of the central detector. The multiwire proportional chamber has in total about 70,000 wires. The magnetic field is 1 Tesla and points upward on the left hand side of the magnet, as seen from the inside of the ISR, and downward on the right hand side.

of the ISR. A perspective drawing of the SFM facility is shown in Fig. 17. In this drawing the top part of the magnet has been taken away to show the two vacuum chambers, that cross at 14.8°, and the set of multiwire proportional chambers used to detect the charged particles produced in the events selected by the trigger system. The detectors used in this experiment were the two forward telescopes, each equipped with 12 chambers, 1 m high, 2 m wide and having wires spaced 2 mm one from the other. The average magnetic field was 1.0 Tesla, providing a momentum resolution of $\pm 7\%$ for the scattered protons. The large coverage of the chambers allowed an acceptance larger than ~40% for momentum transfers larger than 3 GeV^2. The results are plotted in Fig. 18, which shows that behind the minimum the slope of the cross-section is $b_2 \simeq 1.8$ GeV^{-2}. Around 6.5 GeV^2 there is a kind of break and a third slope $b_3 \simeq 0.9$ GeV^{-2} appears in the range $6 \leq |t| \leq 10$ GeV^2. By using an optical model it was quite natural to expect a second diffraction minimum around 4 or 5 GeV^2. The data exclude this possibility.

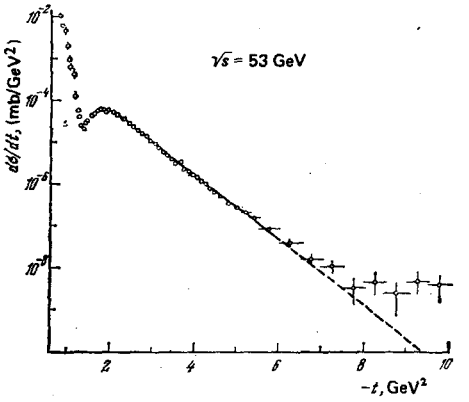

FIG. 18. Proton-proton differential cross section as measured at the SFM by the CERN-Hamburg-Orsay-Vienna collaboration.[23] Around 6 GeV^2 the slope of the differential cross section changes. These results are confirmed by data obtained at Fermilab, and show that there is no second minimum for momentum transfers smaller than 10 GeV^2.

5. WHAT HAVE WE LEARNED FROM HADRON-PROTON SCATTERING?

As anticipated, the higher energy and intensity of proton beams and the use of the proton-proton Intersecting Storage Ring have resulted in the availability of proton-proton data of high quality. Experiments on scattering of other hadrons by protons and neutrons are less abundant and precise, so that in the discussion of the general feature of high energy diffraction the proton-proton channel plays a dominant role. With this in mind, let us now discuss the main findings.

5.1. Energy dependence of total cross sections

Two features are apparent from Figs. 5 and 7. The differences of the cross sections for particles and antiparticles scattered by protons decrease rapidly with energy and all cross sections have a shallow minimum around 50 GeV/c, with the exception of the K^+p channel.

The convergence of particle and antiparticle cross section towards a common value is in agreement with a fundamental theorem due to Pomeranchuk,[24] that follows from very general hypotheses on the energy dependence of the scattering amplitudes. The energy behavior of the differences plotted in Fig. 7 can be understood in the framework of an exchange picture of high energy hadron-hadron collisions. In quantum electrodynamics the basic process used to describe electron-proton scattering is the exchange of a virtual photon between the two colliding particles (Fig. 19a). The Coulomb amplitude describing this process appears in Eq. (24): α is the coupling constant between charges and photons, and $1/p^2\theta^2 = 1/t$ is the factor describing the propagation of the virtual photon. The simplicity of this formula follows from two facts: (i) in electrodynamics the coupling constant is small and (ii) there is only one virtual particle that, through its exchange, gives rise to electromagnetic forces. In the case of strong interactions, the coupling constant is large and, moreover, many virtual hadrons may be exchanged. Still the application of ideas due originally to Regge[25] allows us to use a relatively simple picture of hadron collisions. In this approach the exchange of particles having the same quantum numbers but different spins are all lumped together as a contribution of what is called a "Regge trajector". The graph of Fig. 19b thus represents the amplitude caused by the exchange of all the virtual hadrons lying on the same trajectory R. This averaging procedure over many elementary processes leads to a simple energy dependence for the amplitude:[25]

$$f_R = F(t)\left(\frac{s}{s_0}\right)^{\alpha(t)-s} \qquad (s_0 = 1\text{GeV}^2). \tag{28}$$

Here we cannot discuss the t-dependence of the complex factor $F(t)$ but we direct our attention to the power dependence of the Regge amplitude. This dependence is different at different values of the momentum transfer and is determined by the Regge trajectory $\alpha(t)$. The trajectory is fixed, for small values of t, by the masses of the particles that are connected by the trajectory in a single family and thus the energy dependence of the amplitude of Eq. (28) is well defined. Due to the optical theorem [Eq. (10)], the expected energy dependence of the total cross section is:

$$\sigma_t = \frac{2h}{\pi}\left[\operatorname{Im} F_1(0)\left(\frac{s}{s_0}\right)^{\alpha_1(0)-1} + \operatorname{Im} F_2(0)\left(\frac{s}{s_0}\right)^{\alpha_2(0)-1} + \ldots\right], \tag{29}$$

where $\alpha_1(0) > \alpha_2(0) > \alpha_3(0)$ etc. and the sum is extended to all Regge trajectories that can be exchanged between the two hadrons without violating the known conservation laws. To obtain an asymptotically constant total cross section, the first Regge trajectory should have $\alpha_1(0) = 1$. The data indicate that all cross-sections rise with energy and that to fit them one needs $\alpha_1(0) \approx 1.05$. The trajectory with "intercept" $\alpha(0) \approx 1$, that determines the very high energy behavior of the total cross sections, has been named "Pomeron". Indeed, having the largest intercept, it dominates asymptotically for $s \to \infty$ and, being equally coupled to particles and antiparticles, automatically guarantees the validity of Pomeranchuk theorem. The secondary trajectories have a smaller intercept and the difference between particle and antiparticle total cross sections should behave as

$$\Delta\sigma_t = \left(\frac{s}{s_0}\right)^{\alpha_2(0)-1}. \tag{30}$$

The data of Fig. 7 show that the expectation of a power behavior is met. The values of the power are consistent with the figures that one can predict for $\alpha_2(0)$ from the known values of the masses of the particles that lie on the secondary trajectories. In summary, from an exchange point of view the data on total cross sections point to a Pomeron trajectory having an intercept larger than 1 and are in agreement with the expected contributions of the secondary trajectories.

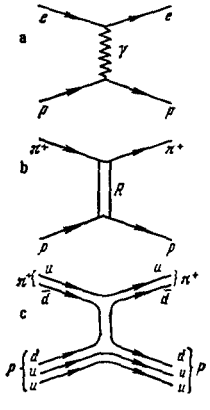

FIG. 19. (a) Electron-proton scattering is due to the exchange of a virtual photon. (b) From the point of view introduced by Chew and Frautschi,[25] pion-proton scattering is mediated by the exchange of a set of particles having the same quantum numbers but different spins. One of this set is called "Reggeon". The figure depicts the exchange of a Reggeon R. (c) From the point of view of the constituent quarks, the exchange of a Reggeon is represented as the annihilation and the simultaneous creation of a quark-antiquark pair.

The Pomeron contribution in the exchange picture is what we have called "diffraction scattering" in the optical picture discussed in the previous sections. Indeed, it is essentially imaginary and dominates at high energy. From the point of view of the quark structure, this contribution is expected to have a strength proportional to the overall number of quarks and antiquarks in the projectile hadron.[26] To understand this result it

is enough to assume that (i) in a hadron-hadron scattering the quark-quark forward amplitudes add and that (ii) the amplitudes dominating at very high energy are all equal, independently of the nature of the interacting quarks. In this picture the contribution of the secondary Regge trajectories is related to the annihilation of the antiquarks of the incoming hadron with the quarks of the target proton and is proportional to the number of possible combinations (see Fig. 19c). These two terms give a *three parameter* description of the total cross sections with an accuracy of the order of 15%. A few years ago Lipkin noted that the addition of a third term containing two other parameters could improve the accuracy by an order of magnitude.[27] The proposed universal parametrization for the hadron-proton (Hp) cross section is compared with the data in Fig. 5 and reads

$$\frac{\sigma(Hp)}{1} = 6.50 N_q^H x^{0.13} + 1.75 (N_d^H + 2N_{\bar{u}}^H) x^{-0.50} + 2.20 N_q^H N_{ns}^H x^{-0.30}, \quad (31)$$

where:

$x = p_{1ab}/(20\ \text{GeV}/c) \approx s$ [see Eq. (12)]

N_q^H = total number of quarks in H

N_{ns}^H = total number of nonstrange quarks and antiquarks in H

$N_{\bar{d}}^H$ = number of $\bar{d}$ antiquarks in H

$N_{\bar{u}}^H$ = number of $\bar{u}$ antiquarks in H.

The first and second terms of Eq. (31) are the quark model recipes for the Pomeron and Regge contributions. The third term decreases slowly with energy and can be considered as due to a second Pomeron with intercept $\alpha(0) \approx 0.8$.

We may conclude this argument by stressing that measurements of the total cross section are experiments at zero momentum transfer, i.e. that they belong to the class of experiments in which it is impossible to obtain *directly* information on the internal structure of hadrons. However, the available data are consistent with a quark-quark picture supplemented by some simple hypotheses. Another model, that considers the "glue" as an active agent in strong interactions, will be described in Section 5.3. It describes elastic scattering data well, but does not give simple expressions for the total cross sections. Both models have attractive features, but clearly the final answer has not been reached.

A relevant question in connection with the energy dependence of the total cross sections is: what is their behavior at energies even larger than the ones attainable at the ISR? A general theorem due to Froissart[28] states than an asymptotic power law, such as the one that appears in Eq. (31), is not compatible with causality. According to this theorem a hadron-hadron cross section cannot increase faster than $(\ln s)^2$. We are, however, very far from "asymptotia" and it can be shown that the observed increasing cross sections have nothing to do with approaching the saturation limit set by Froissart. Thus the only reliable information on higher energy proton-proton cross sections comes from the already discussed accurate measurement of the ratio ρ performed at the ISR by the CERN-Rome Collaboration.[16] A dispersion relation connects ρ to an integral over the total cross sections; at a fixed energy such an integral relation states, roughly speaking, that ρ is proportional to the derivative of the cross section as a function of $\ln s$. This explains why an accurate measurement of the forward real part constrains very strongly the behavior of σ_t. The results of a simultaneous fit to all the available data on ρ and σ_t are shown in Fig. 20.[16] In the fit the high energy behavior of σ_t has been varied. As a result one has obtained the shaded areas, that are one standard deviation limit for the high energy behavior of both quantities. It is seen that the proton-proton cross section continues to increase above the measured range up to *at least* $\sqrt{s} \simeq 300$ GeV, that corresponds to $p_{1ab} \approx 50.000$ GeV/c, where it should reach 55 mb.

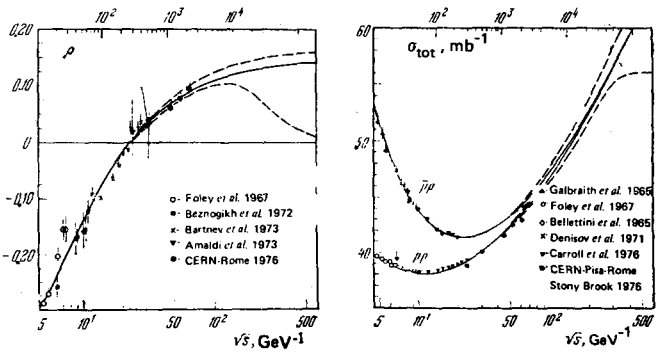

FIG. 20. The round points represent the most recent measurements of ρ and σ_t performed at the ISR. The continuous curves are *simultaneous* fits to the energy dependence of the ratio ρ and the total cross section σ_t, taking into account the dispersion relation that connects these two quantities. The accurate determination of ρ at the ISR fixes the behavior of σ_t at much larger energies, so that one can say that the total cross section increases up to at least 350 GeV in the center of mass. In this context, the dashed areas represent the one standard deviation regions, such that there is a 68% probability that the quantities ρ and σ_t do not lie outside them.

5.2. Elastic cross sections and hadron-proton absorptiveness

Elastic cross sections are obtained by integrating the differential cross section $d\sigma/dt$. Accuracies of the order of a few percent may be obtained when the integral is extended up to momentum transfers of the order of 1 GeV^2. The existing data are plotted in Fig. 21 together with the energy dependence of the ratio σ_{el}/σ_t. The most striking feature is that all channels reach a constant value of σ_{el}/σ_t by 100 GeV. Especially impressive is the fact that the value 0.18 for proton-proton scattering is observed from 10 GeV to ISR energies.

In the diffraction picture the ratio $2\sigma_{el}/\sigma_t$ is a measure of the average hadron-hadron absorptiveness A [see Eq. (6)]. Above about 10 GeV the data of Fig. 21 give $A \simeq 0.26$ in the $\pi^+ p$ and $K^+ p$ channels and $A \simeq 0.36$ in the pp and $\bar{p}p$ channels. These numbers are small, indicating that hadrons are relatively transparent to one another. Moreover, their absorptiveness does not vary appreciably with energy, in spite of the fact that the total cross sections increase.

A constant absorptiveness is compatible with an in-

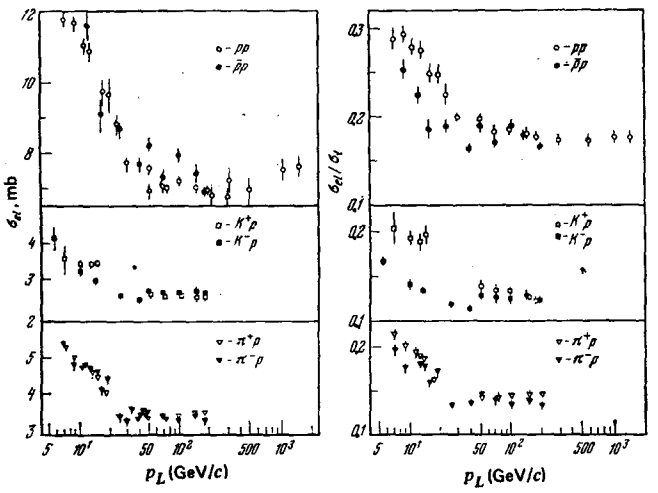

FIG. 21. Compilation of data on the energy behavior of the elastic cross section and on the ratio σ_{el}/σ_t.[29] It is worth recalling that in a simple diffraction picture the *average* hadron-hadron absorptiveness equals $2\sigma_{el}/\sigma_t$ [Eq. (6)].

creasing total cross section only if the interaction radius R increases with energy. This is indeed the case, as is indicated by the $(12 \pm 3)\%$ increase of the forward slope observed for the proton-proton channel in the ISR energy range, i.e. when $\sqrt{s}$ increases from 23 to 63 GeV. In the same interval the total cross section increases by $(11 \pm 2)\%$ and, as discussed in Section 4.3, the position of the minimum in the elastic cross section moves by $(14 \pm 3)\%$. All these data are thus consistent with the picture that *in the ISR energy range the proton-proton absorptiveness stays constant, while the interaction radius increases by about* 6%. Similar phenomena are also appearing in the other channels, pointing to the conclusion that at high energy strong interactions are such that hadrons are far from being fully absorbing bodies. When the energy increases their absorptiveness remains sensibly constant, a fact that came as a surprise just because they are not fully absorbing. The interaction radius which increases more or less as the logarithm of energy gives rise to the phenomenon of the rising hadron-hadron cross sections. All this is at variance with the theoretical expectations of the sixties, when Regge models predicted constant cross sections with an increasing interaction radius and a decreasing absorptiveness.

More detailed analyses of the differential cross section data are possible as a result of which one can obtain the shape of the absorptiveness profile, and not only its average value. They are summarized in a recent review paper.[30] These more refined analyses arrive at the same conclusion: the hadron-hadron absorptivness profiles scale with energy in such a way that the central absorption stays constant while the average radius increases.[31] Now the question that arises is: why do the inelastic processes, that in the optical picture are responsible for absorption and for the consequent diffraction, give rise to this very special behavior? In the exchange picture the same question is expressed in different words: why does the Pomeron behave in the presently attainable energy range as if its intercept were larger than 1 by about 5%. Two languages but a single question to which we do not have, for the moment, a convincing answer. Moreover an understanding of this difficult dynamical problem of the strong interactions should be reached by taking into account the composite structure of the hadrons that was discussed in Section 1 and that is consistently indicated by experiments on the weak and electromagnetic forces.

5.3. Diffraction scattering and hadron structure

As has been stressed repeatedly, low momentum transfer experiments cannot give direct information on the internal structure of the interacting particles. On the other hand, since lepton-hadron scattering has shown that hadrons have a composite structure, it is legitimate to ask whether the diffraction data described above can be coherently interpreted in the framework of the quark model introduced in Section 1. Many attempts have been made in this direction. We shall concentrate on the approach due to Fialkowski, Pokorski and Van Hove,[31,32] that has the merit of being intuitively simple and of connecting with few hypotheses a large amount of sparse information.

Let us first list the four main facts one would like to correlate.

(i) As is shown above, it follows from the data on hadron-hadron elastic scattering that the central absorption is practically constant with energy, while the interaction radius increases linearly with $\ln s$. By making use of a particle language, let us indicate by a the minimum distance of approach of the two colliding hadrons. The absorption A is in general a function of the "impact parameter" a, and the experiments summarized above tell us that at high energy the functional dependence is very simple.

$$A(a) \approx A\left[\frac{2}{R(s)}\right], \tag{32}$$

This property has been named "geometrical scaling"[33] because it implies that with increasing energy the absorptiveness profile maintains its shape, but scales in radius. Eq. (32) gives rise both to the logarithmic increase with energy of the slope parameter b (Eq. (27)) and to the increasing total cross section.

(ii) The value of the central absorption $A(0)$ is relatively small. In the proton-proton case the analysis performed on the data shows that for $23 \leq \sqrt{s} \leq 63$ GeV one has $A(0) \simeq 0.75$. This value is far from the maximum allowed $A(0) = 1.0$, that corresponds to full absorption of the proton waves at impact parameter equal to zero. For full absorption the energy dependence of the central absorptiveness would be a trivial statement, since $A(0)$ cannot be greater than 1. But one is far from this condition and geometrical scaling is a dynamical fact to be understood.

(iii) The elastic cross section has a minimum at $|t| \simeq 1.4$ GeV^2 and above this minimum the slope is small: $b \simeq 1.8$ GeV^{-2}. Moreover, there is a change of slope around $|t| \simeq 8$ GeV^2 but no other minimum is observed.

(iv) Elastic diffraction scattering is due to the absorption caused by the large cross section for the inelastic processes. For this reason it is often said that at high energy elastic scattering is the shadow of the

inelastic channels. An important phenomenon, that is out of the scope of the present article, is also caused by the very presence of the inelastic channels: *inelastic diffraction scattering*. Its nature can be understood in rather simple terms; a more complete discussion can be found in Ref. 30. Due to their composite nature, the colliding hadrons can be described as linear superpositions of many states having the same intrinsic quantum numbers. During the interaction these "diffractive eigenstates" give rise to different inelastic processes, so that each of them is, in general, absorbed in a different way. After the interaction, the various diffractive eigenstates are no longer present with the same weights so that their superposition gives back the initial hadrons (elastic diffraction scattering) plus other hadrons, having the same intrinsic quantum numbers but different masses (inelastic diffraction scattering). Experiment shows that at high energy the inelastic diffractive cross section σ_D is almost equal to the elastic cross section σ_{el}. Only recently has it been realized that this is a surprising result.[34] Indeed, elastic diffraction is directly given by the absorption profiles of the diffractive eigenstates while inelastic diffraction is determined by the *differences* between these profiles. These differences have to be large, if σ_D has to be equal to σ_{el}. This means that the diffractive eigenstates have to group in two categories, some of them being heavily absorbed while others are almost undisturbed by the interaction. In this way at least some of the profile differences may get a chance to be large. Since here it is not possible to go into more detail, it is enough to stress that any dynamical model of diffraction has to explain why the diffractive eigenstates behave so differently from one another.

This remark concludes the list of the four facts one would like to understand from a unified point of view. The quark-glue model of Fialkowski, Pokorski and Van Hove regards hadrons as built up of quarks and "glue", this being responsible for the quark-quark forces. While electromagnetic and weak interactions act only on the quarks, the glue is responsible for the hadronic inelastic processes. In a hadron-hadron collision the quarks fly through, thus giving rise to the so-called leading particles, while the glue interacts producing the bulk of the secondary hadrons. The authors have shown that the momentum distribution of the quarks inside a hadron derived from lepton experiments is naturally related to the measured distribution of the leading particles. Moreover, the model produces large variations of absorptiveness for the diffractive eigenstates to account for the observation discussed above under point (iv). This is related to the fact depicted in Fig. 22a: the glue-glue impact parameter a_g is *not* equal to the hadron-hadron impact parameter a. By assuming that the absorption is complete for central glue-glue collisions, one obtains the needed wide spectrum of absorptions. Indeed, for a given hadron-hadron impact parameter a, when $a_g=0$ one has $A=1$, while A decreases rapidly to zero for increasing a_g.

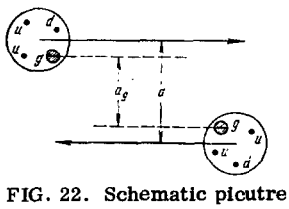

FIG. 22. Schematic picutre of a proton-proton interaction in the quark-glue model: a_g and a are the glue-glue and proton-proton impact parameters. The black dots represent the quarks determining the intrinsic quantum numbers of the colliding protons.

In this model the energy independence of $A(a=0)$ (point (ii)) follows from the fact that for $a=0$ the glue impact parameter a_g is not fixed. By averaging over the glue-glue impact parameter with a gaussian distribution in a_g and with $A(a_g=0)=1$, Van Hove and Fialkowski have shown that the proton-proton central absorption can be consistently made equal to 0.75. On the other hand the geometrical scaling properties of the absorptiveness profile [point (i)] do not come out automatically, and one has to assume that the glue-glue interaction radius increases with energy.

Finally, it is enough to assume that the glue-glue absorption is maximal not only at $a_g=0$ but also in a small but finite interval around this point[32] to give a very good description of the elastic cross-section for $0 \leq |t| \lesssim 8$ GeV^2 [point (iii)].

In this model the glue is responsible for strong interaction collisions. A few very natural assumptions lead to a coherent understanding of the four facts described above. However, in order to account for the successes of the quark model relations for the total cross sections (and in particular for Eq. (31)) one should furthermore assume a dependence of the glue density on the number and properties of the quarks. Clearly we are far from a deep understanding of elastic (and inelastic) hadronic diffraction scattering at high energy. But the way is already open to illuminating relations between this physics and the information on the structure of the hadrons continuously gathered from experiments involving weak and electromagnetic forces.

[1]Yu. B. Bushnin *et al.*, Phys. Lett. **B29**, 48 (1969); J. V. Allaby *et al.*, Phys. Lett. **B30**, 500 (1969); J. V. Allaby *et al.*, Yad. Fiz. 12, 538 (1970) [Sov. J. Nucl. Phys. **12**, 295 (1970)].
[2]G. Giacomelli, Prog. Nucl. Phys. 12, 77 (1970).
[3]K. Johnsen, Nucl. Instrum. Meth. **108**, 205 (1973).
[4]S. van der Meer, CERN Internal Report ISR-PO/68-31 (1968).
[5]CERN-Pisa-Roma-Stony Brook Collaboration, Phys. Lett. **62B**, 460 (1976).
[6]U. Amaldi *et al.*, Phys. Lett. **B44**, 112 (1973).
[7]S. R. Amendolia *et al.*, Phys. Lett. **B44**, 119 (1973).
[8]U. Amaldi *et al.*, Submitted to Nuovo Cimento (1977).
[9]K. J. Foley *et al.*, Phys. Rev. Lett. **19**, 857 (1967).
[10]S. P. Denisov *et al.*, Nucl. Phys. **B56**, 1 (1973).
[11]A. S. Carroll *et al.*, Phys. Lett. **B61**, 303 (1976).
[12]L. F. Kirillova *et al.* Yad. Fiz. 1, 533 (1965) [Sov. J. Nucl. Phys. 1, 379 (1965)].
[13]Y. K. Akimov *et al.*, Zh. Eksp. Teor. Fiz. **48**, 767 (1965) [Sov. Phys. JETP **21**, 507 (1965)]; Y. K. Akimov *et al.* J. Nucl. Phys. **4**, 88 (1966); G. G. Beznogikh *et al.*, Phys. Lett. **30B**, 274 (1969); ibid, **43B**, 85 (1973).
[14]G. Beznogikh *et al.*, Phys. Lett. **39B**, 411 (1972).
[15]V. Bartenev *et al.*, Phys. Rev. Lett. **29**, 1755 (1972); V. Bartenev *et al.*, Phys. Rev. Lett. **31**, 1088 (1973); V. Bartenev *et al.*, Phys. Rev. Lett. **31**, 1367 (1973).
[16]U. Amaldi *et al.*, Phys. Lett. **43B**, 231 (1973); U. Amaldi *et al.*, Phys. Lett. **66B**, 390 (1977).

[17]A. E. Taylor *et al.*, Phys. Lett. **14**, 55 (1965); L. F. Kirillova *et al.*, Zh. Eksp. Teor. Fiz. **50**, 76 (1966) [Sov. Phys. JETP **23**, 52 (1966)]; K. J. Foley *et al.*, Phys. Rev. Lett. **19**, 857 (1967); K. J. Foley *et al.*, Phys. Rev. **181**, 1775 (1969); G. G. Bezognikh *et al.*, Phys. Lett. **B39**, 411 (1972); A. A. Vorobyov *et al.*, Phys. Lett. **B41**, 639 (1972); N. N. Govuron *et al.*, El-7552-Dubna, JINR (1973); V. D. Apokin *et al.*, Phys. Lett. **B56**, 391 (1975); R. K. Carnegie *et al.*, Phys. Lett. **B59**, 308 (1975); C. Ankenbrandt *et al.*, Fermilab Conf. 75/61 Exp 7100.069 (1975); P. Jenni *et al.*, Nucl. Phys. **B94**, 1 (1975); P. Jenni *et al.*, Nucl. Phys. **B105**, 1 (1976); P. Baillon *et al.*, Nucl. Phys. **B105**, 365 (1976); P. Baillon *et al.*, Nucl. Phys. **B107**, 189 (1976); V. D. Apokhin *et al.*, IHEP 76-6 (1976); P. Jenny *et al.*, CERN/EP/PHYS 77-21 (1977).
[18]R. E. Hendrick and B. Lautrup, Phys. Rev. D **11**, 529 (1975); R. E. Hendrick *et al.*, Phys. Rev. D **11**, 536 (1975).
[19]Fermilab Single Arm Spectrometer Group, Fermilab-Pub-76/66-Exp 7100.096 (1977), submitted to Phys. Rev. D.
[20]U. Amaldi *et al.*, Phys. Lett. **B44**, 116 (1971); G. Beznogikh *et al.*, Phys. Lett. **B43**, 85 (1973); V. Bartenev *et al.*, Phys. Rev. Lett **31**, 1088 (1973); Yu. M. Antipov *et al.*, Nucl. Phys. **B57**, 333 (1973); A. A. Derevshchikov *et al.*, Phys. Lett. **B48**, 367 (1974); S. Nurushev, Proc. Int. Conf. High Energy Phys. 17th, ed. J. R. Smith, **1**, 25 (1974), Didcot, Engl. Rutherford Lab.; Fermilab Single Arm Spectrometer Group, Phys. Rev. Lett. **35**, 1195 (1975); C. W. Akerlof *et al.*, Phys. Rev. Lett. **35**, 1406 (1975).
[21]A. R. Clyde, University of Cal. Rad. Lab. Report UCRL 16275 (1976); J. V. Allaby *et al.*, Nucl. Phys. **B52**, 316 (1973); C. W. Akerlof *et al.*, Phys. Lett. **B59**, 197 (1975).
[22]N. Kwak *et al.*, Phys. Lett. **B58**, 233 (1975).
[23]H. de Kerret *et al.*, Phys. Lett. **B62**, 363 (1976); H. de Kerret *et al.*, Phys. Lett., to be published.
[24]I. Ia. Pomeranchuk, Zh. Eksp. Teor. Fiz. **34**, 725 (1958) [Sov. Phys. JETP **7**, 499 (1958)].
[25]T. Regge, Nuovo Cimento **14**, 951 (1959); **18**, 947 (1960); G. F. Chew and S. Frantschi, Phys. Rev. Lett. **8**, 41 (1962).
[26]E. M. Levin and L. L. Frankfurt, Pis'ma Zh. Eksp. Teor. Fiz. **2**, 105 (1965) [JETP Lett. **2**, 65 (1965)]; H. J. Lipkin, Phys. Rev. Lett. **16**, 1015 (1966).
[27]H. J. Lipkin, Phys. Rev. D **11**, 1827 (1975).
[28]M. Froissart, Phys. Rev. **123**, 1053 (1961); A. Martin, Nuovo Cimento **42**, 930 (1966).
[29]P. J. Carlson *et al.*, Landolt-Börnstein New Series, Vol. 7, (1973), ed. K. H. Hellwege, Berlin:Springer; Particle Data Group "NN and ND Interactions—A Compilation" UCRL = = 20000NN. (1970); D. R. O. Mossison, "Total Inelastic Cross Sections" CERN/D.PRII/PHYS 74-38 (1974); High Energy Reactions Analysis Group, CERN/HERA 72-2, CERN HERA 73-1.
[30]U. Amaldi, M. Jacob and G. Matthiae, Annu. Rev. Nucl. Sci. **26**, 385-456 (1976).
[31]S. Pokorski and L. Van Hove, Acta Phys. Pol. **B5**, 229 (1974); L. Van Hove and S. Pokorski, Nucl. Phys. **B36**, 243 (1975); L. Van Hove, Acta Phys. Pol. **B7**, 339 (1976); L. Van Hove and K. Fialkowski, Nucl. Phys. **B107**, 211 (1976).
[32]L. Van Hove, Nucl. Phys. **B122**, 525 (1977).
[33]J. Dias de Deus, Nucl. Phys. **B59**, 231 (1973); V. Barger, Proc. Int. Conf. High Energy Phys. 17th, **1**, 200 (1974), ed. J. R. Smith, Didcot, Engl.: Rutherford Lab.
[34]K. Failkowski and H. I. Miettinen, Nucl. Phys. **B103**, 247 (1976).